



UNIVERSITY OF LEEDS

This is a repository copy of *c-Rel orchestrates energy-dependent epithelial and macrophage reprogramming in fibrosis*.

White Rose Research Online URL for this paper:
<https://eprints.whiterose.ac.uk/168369/>

Version: Accepted Version

Article:

Leslie, J, Macia, MG, Luli, S et al. (39 more authors) (2020) c-Rel orchestrates energy-dependent epithelial and macrophage reprogramming in fibrosis. *Nature Metabolism*, 2 (11). pp. 1350-1367. ISSN 2522-5812

<https://doi.org/10.1038/s42255-020-00306-2>

Copyright © 2020, The Author(s), under exclusive licence to Springer Nature Limited. This is an author produced version of a paper published in *Nature Metabolism*. Uploaded in accordance with the publisher's self-archiving policy.

Reuse

Items deposited in White Rose Research Online are protected by copyright, with all rights reserved unless indicated otherwise. They may be downloaded and/or printed for private study, or other acts as permitted by national copyright laws. The publisher or other rights holders may allow further reproduction and re-use of the full text version. This is indicated by the licence information on the White Rose Research Online record for the item.

Takedown

If you consider content in White Rose Research Online to be in breach of UK law, please notify us by emailing eprints@whiterose.ac.uk including the URL of the record and the reason for the withdrawal request.



eprints@whiterose.ac.uk
<https://eprints.whiterose.ac.uk/>

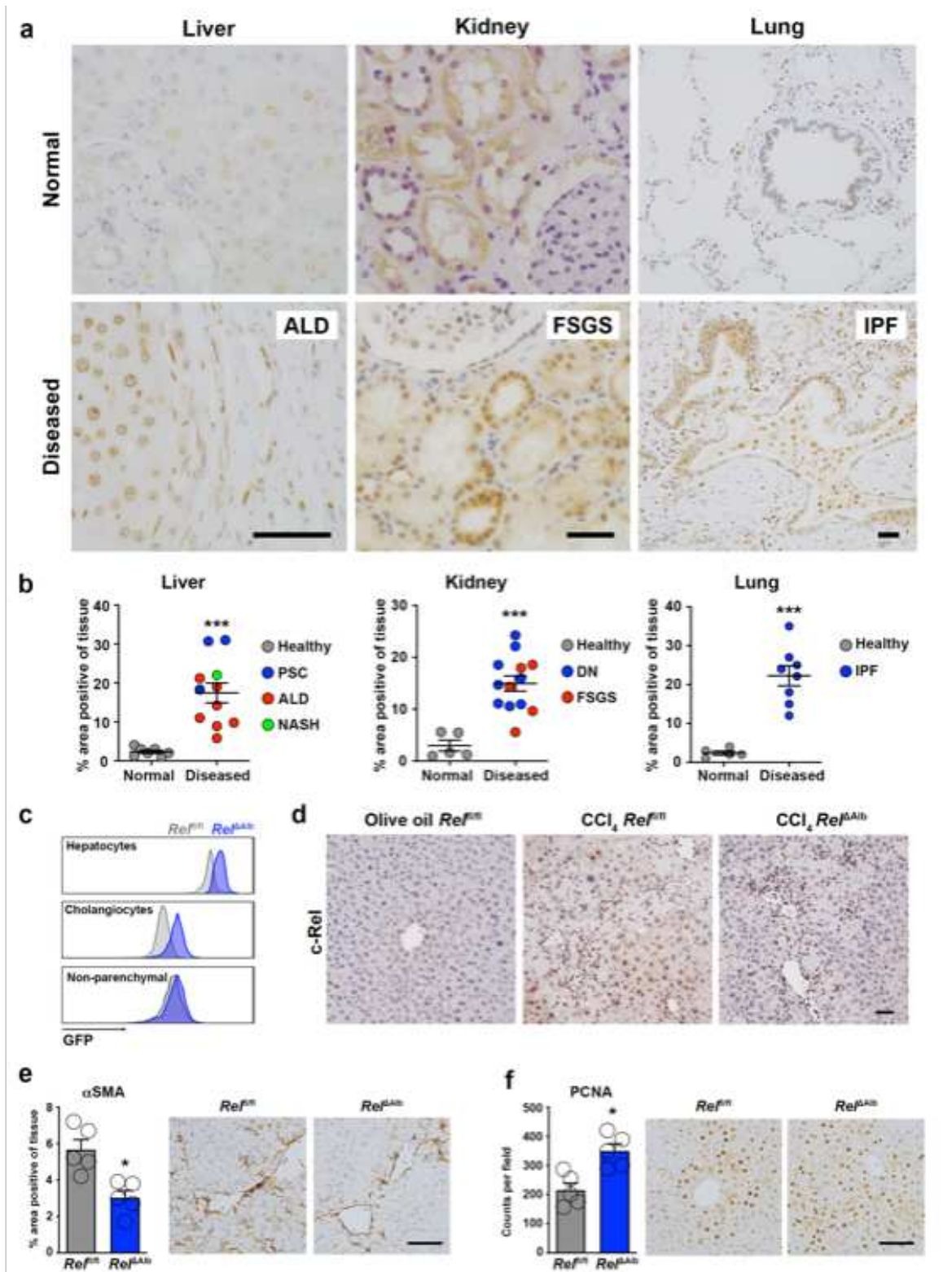


Figure 1. c-Rel is a feature of chronic liver, kidney and lung disease in humans and epithelial c-Rel signalling regulates hepatic fibrogenesis and regeneration in mice

(a) Representative images show c-Rel staining in normal and diseased liver, lung and kidney sections. (b) Graphs show average percentage area of c-Rel stained tissue in normal liver, lung and kidney sections compared to diseased human liver (alcoholic liver disease (ALD), primary sclerosing cholangitis (PSC) and non-alcoholic steatohepatitis (NASH)), diseased kidney (focal segmented glomerular sclerosis (FSGS) and diabetic nephropathy (DN)) or lung disease, idiopathic pulmonary fibrosis (IPF). Data are mean \pm s.e.m. in 7 healthy and 11 diseased patient tissue for liver (p value = 0.0003), 5 healthy and 13 diseased patient tissue for kidney (p value = 0.0002) and 5 healthy and 8 diseased patient tissue for lung (p value <0.0001). (c) FACS plot showing the Mean Fluorescence Intensity (MFI) of GFP in hepatocytes, cholangiocytes (EPCAM+) and non-parenchymal (EPCAM-) cells from the liver of *Rel^{fl/fl}* (grey) and *Rel ^{Δ Alb}* (blue) mice. (d) Representative images show c-Rel staining 5 mice/group in olive oil *Rel^{fl/fl}* mice and CCl₄ injured *Rel^{fl/fl}* and *Rel ^{Δ Alb}* mice. (e-f) Histological assessment and representative images of (e) α SMA (p value = 0.005) and (f) PCNA (p value = 0.005) stained liver sections in acute CCl₄ injured *Rel^{fl/fl}* and *Rel ^{Δ Alb}* mice. Data are mean \pm s.e.m. in 5 mice/group. Scale bars equal 50 microns. All P values were calculated using a unpaired two-sided T test (* P <0.05, *** P <0.001).

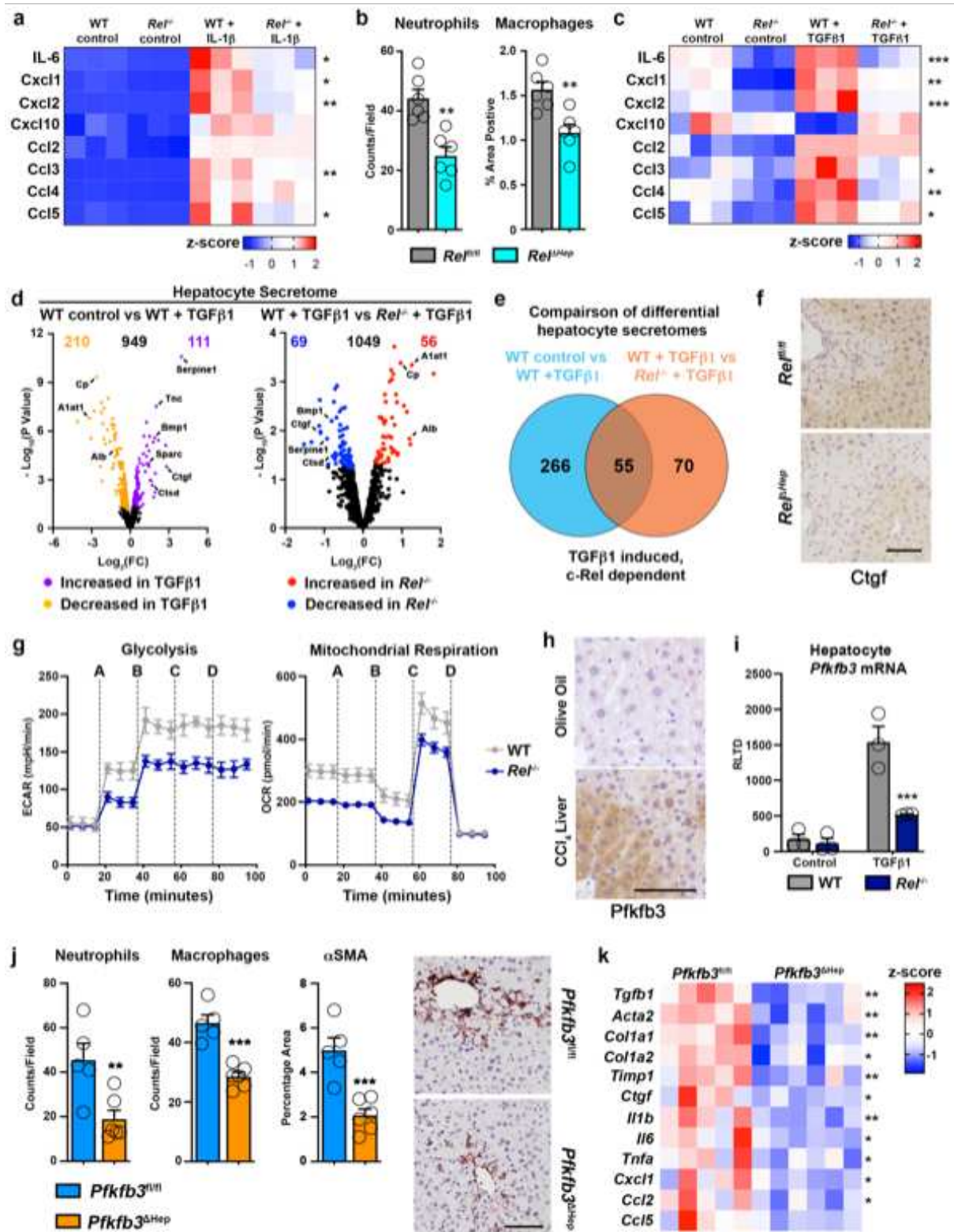


Figure 2. c-Rel signalling regulates epithelial inflammatory responses via regulation of Pfkfb3 (a) Heatmap showing secreted IL6, Cxcl1, Cxcl2, Cxcl10, Ccl2, Ccl3, Ccl4 and Ccl5, measured by MSD in the media of hepatocytes isolated from WT

and *Rel*^{-/-} mice and stimulated ± IL-1β. (b) Graph shows quantification of neutrophil (p value = 0.0012) and macrophage (p value = 0.0039) numbers in the liver of acute CCl₄ injured *Rel*^{fl/fl} and *Rel*^{ΔHep} mice. (c) Heatmap showing secreted IL6, Cxcl1, Cxcl2, Cxcl10, Ccl2, Ccl3, Ccl4 and Ccl5, measured by MSD in the media of hepatocytes isolated from WT and *Rel*^{-/-} mice and stimulated ± TGFβ1. (d) Volcano plots show differentially expressed proteins detected by proteomic analysis of the secretome of WT control and WT TGFβ1 treated hepatocytes (left) and TGFβ1 treated WT and *Rel*^{-/-} hepatocytes (right). (e) Venn diagram shows the number of differentially expressed proteins in TGFβ1 treated WT hepatocytes compared to control WT hepatocytes (Blue) and number of differentially expressed proteins in TGFβ1 treated WT hepatocytes compared to TGFβ1 treated *Rel*^{-/-} hepatocytes (Orange). The overlap denotes c-Rel dependent secreted proteins in response to TGFβ1 stimulation. (f) Representative images show CTGF staining in the liver of 6 mice/group acute CCl₄ injured *Rel*^{fl/fl} and *Rel*^{ΔHep} mice. (g) Graphs show seahorse analysis of glycolysis (extracellular acidification rate, ECAR) and mitochondrial respiration (oxygen consumption rate, OCR) in WT and *Rel*^{-/-} hepatocytes stimulated ± TGFβ1. Where A-D vertical lines refer to the administration of the following compounds: A – Glucose, B – Oligomycin, C- Pyruvate and FCCP, D – Rotenone and Antimycin A. (h) Representative images show Pfkfb3 staining in a minimum of 5 mice/group of olive oil control and CCl₄ injured liver. (i) Graph shows mRNA expression of *Pfkfb3* in WT and *Rel*^{-/-} hepatocytes stimulated ± TGFβ1. (p value = 0.0008) (j) Quantification of neutrophil (p value= 0.0097) and macrophage (p value = 0.0002) numbers and histological assessment and representative images of αSMA (p value = 0.001) stained liver sections in acute CCl₄ injured *Pfkfb3*^{fl/fl} and *Pfkfb3*^{Δhep} mice. P values were calculated using a unpaired two-sided T test. (k) Heatmap shows mRNA levels of

fibrogenic genes; *Tgfb1*, *Acta2*, *Col1a1*, *Col1a2*, *Timp1*, *Ctgf* and inflammatory genes; *Il1b*, *Il6*, *Tnfa*, *Cxcl1*, *Ccl2* and *Ccl5* in acute CCl₄ injured *Pfkfb3^{fffl}* and *Pfkfb3^{Δhep}* mice. Data in graphs are mean ± s.e.m. in 7 mice/genotype (c), n=5 *Pfkfb3^{fffl}* and n=6 *Pfkfb3^{Δhep}* mice (e), or a minimum of 3 independent cell isolations/condition. Scale bars equal 100 microns. (a, c, i) P values were calculated using a two-way ANOVA with Tukey post-hoc t-test. (b, j, k) P values were calculated using unpaired two-tailed T-test (* P <0.05, ** P <0.01 and ***P<0.001).

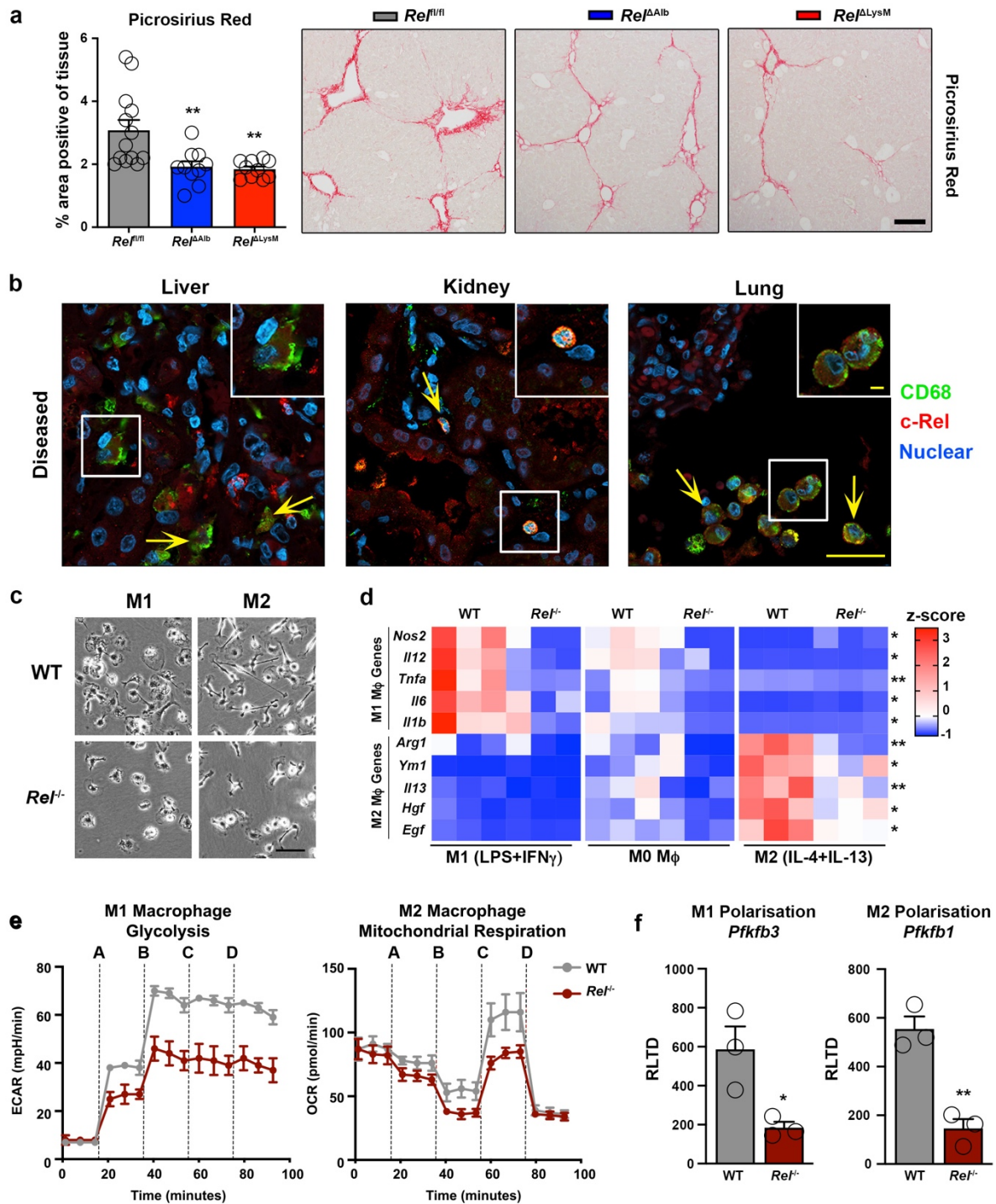


Figure 3. c-Rel signalling in macrophages is pro-fibrogenic and regulates macrophage plasticity

(a) Histological assessment and representative images of Picrosirius red (collagen) stained liver sections in chronic CCl_4 injured in $Re1^{fl/fl}$, $Re1^{\Delta Alb}$ (p value = 0.0064) and $Re1^{\Delta LysM}$ (p value = 0.0035) mice. Data are mean \pm s.e.m. in 10 mice/group, scale bar

equals 100 microns. (b) Representative immuno-fluorescence images show c-Rel (red), CD68 (green) and nuclear (blue) staining in human diseased liver (n=11), kidney (n=13) and lung (n=8) sections. Yellow arrows denote co-localisation of c-Rel and CD68. Scale bars equal 20 microns. (c) Representative bright-field images of WT and *Rel^{-/-}* M1 and M2 polarised BMDMs in 3 independent cell isolations. Scale bar = 50 microns (d) Heat map shows mRNA expression of *Nos2*, *Il12*, *Tnfa*, *Il6*, *Il1b*, *Arg1*, *Ym1*, *Il13*, *Hgf* and *Egf* in M0, M1 and M2 polarised WT and *Rel^{-/-}* BMDM respectively. (e) Graphs show glycolysis (extracellular acidification rate, ECAR) and mitochondrial respiration (oxygen consumption rate, OCR) in M1 and M2 polarised WT and *Rel^{-/-}* BMDM respectively. Where A-D vertical lines refer to the administration of the following compounds: A – Glucose, B – Oligomycin, C- Pyruvate and FCCP, D – Rotenone and Antimycin A (f) Graphs show mRNA expression of *Pfkfb3* (p value = 0.029) and *Pfkfb1* (p value = 0.0031) in M1 and M2 polarised WT and *Rel^{-/-}* BMDMs. Data are mean \pm s.e.m of n=3 independent cell isolations. (a, d) P values were calculated using a two-way ANOVA with Tukey post-hoc t-test. (f) P values calculated using an unpaired two-side T test. P values equal *P<0.05 and **P<0.01. Asterisks on heatmaps denote significance between WT and *Rel^{-/-}* macrophages in M1 or M2 responsive genes in line with the M1 or M2 stimulation. There is no significant difference between M0 macrophages from either genotype.

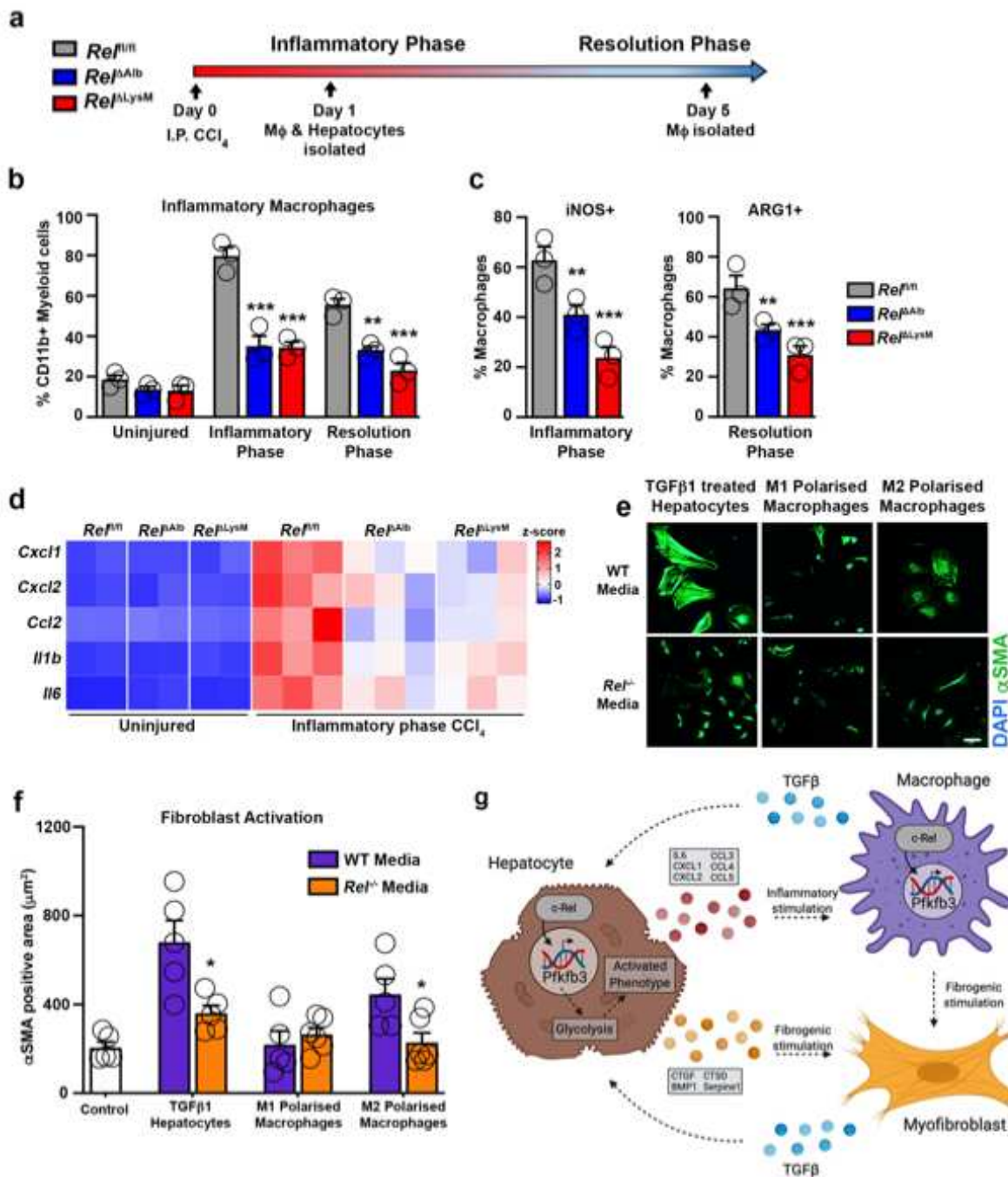


Figure 4. c-Rel regulates pro-fibrogenic epithelial-macrophage crosstalk to accelerates fibroblast activation

(a) Schematic shows *Re1^{fl/fl}*, *Re1^{ΔLysM}* and *Re1^{ΔAlb}* mice receiving CCl₄ mediated acute liver injury. Mice were harvested at day 1 and day 5 post CCl₄ injury during the inflammatory and resolution phases of wound healing (WH) respectively. (b) FACS quantification of the percentage (%) of CD11b^{Hi}F4/80^{Int} inflammatory macrophages in

uninjured liver and during the inflammatory (day 1) (p values = 0.0002 for *Rel^{ΔAlb}* and 0.00012 *Rel^{ΔLysM}* mice) and resolution (day 5) (p values = 0.0037 for *Rel^{ΔAlb}* and 0.0002 *Rel^{ΔLysM}* mice) phases of WH in acute CCl₄ injured *Rel^{fl/fl}*, *Rel^{ΔAlb}* and *Rel^{ΔLysM}* mice. (c) FACS quantification of the percentage (%) of iNOS+ (p values = 0.0033 for *Rel^{ΔAlb}* and 0.0002 *Rel^{ΔLysM}* mice) and ARG1+ (p values = 0.0043 for *Rel^{ΔAlb}* and 0.0001 *Rel^{ΔLysM}* mice) inflammatory macrophages during the inflammatory and resolution phases of WH respectively in acute CCl₄ injured *Rel^{fl/fl}*, *Rel^{ΔLysM}* and *Rel^{ΔAlb}* mice. Data in graphs are mean ± s.e.m of n=4 independent cell isolations. (d) Heatmap shows mRNA expression of inflammatory genes; *Cxcl1*, *Cxcl2*, *Ccl2*, *Il1b* and *Il6* in primary hepatocytes isolated from *Rel^{fl/fl}*, *Rel^{ΔLysM}* and *Rel^{ΔAlb}* mice during the inflammatory phase of WH. (e) Representative immuno-fluorescence images of αSMA (green) and nuclear (blue) staining, scale bar = 50 microns. (f) Graph showing quantification of αSMA stained area (f) in WT hepatic stellate cells cultured in media only (control) or conditioned media from WT or *Rel^{-/-}* hepatocytes treated ± TGFβ1 (p value = 0.0153) or WT or *Rel^{-/-}* M1 and M2 (p value = 0.024) polarised macrophages. Data are mean ± s.e.m of n=3 independent cell isolations. (b, c, f) P values were calculated using a two-way ANOVA with Tukey post-hoc t-test or an unpaired two-tailed t-test (* P <0.05, ** P <0.01 and *** P <0.001). (g) Model shows c-Rel-Pfkfb3 dependent paracrine epithelial-macrophage crosstalk driving fibroblast activation within the fibrogenic niche. Model created using biorender.

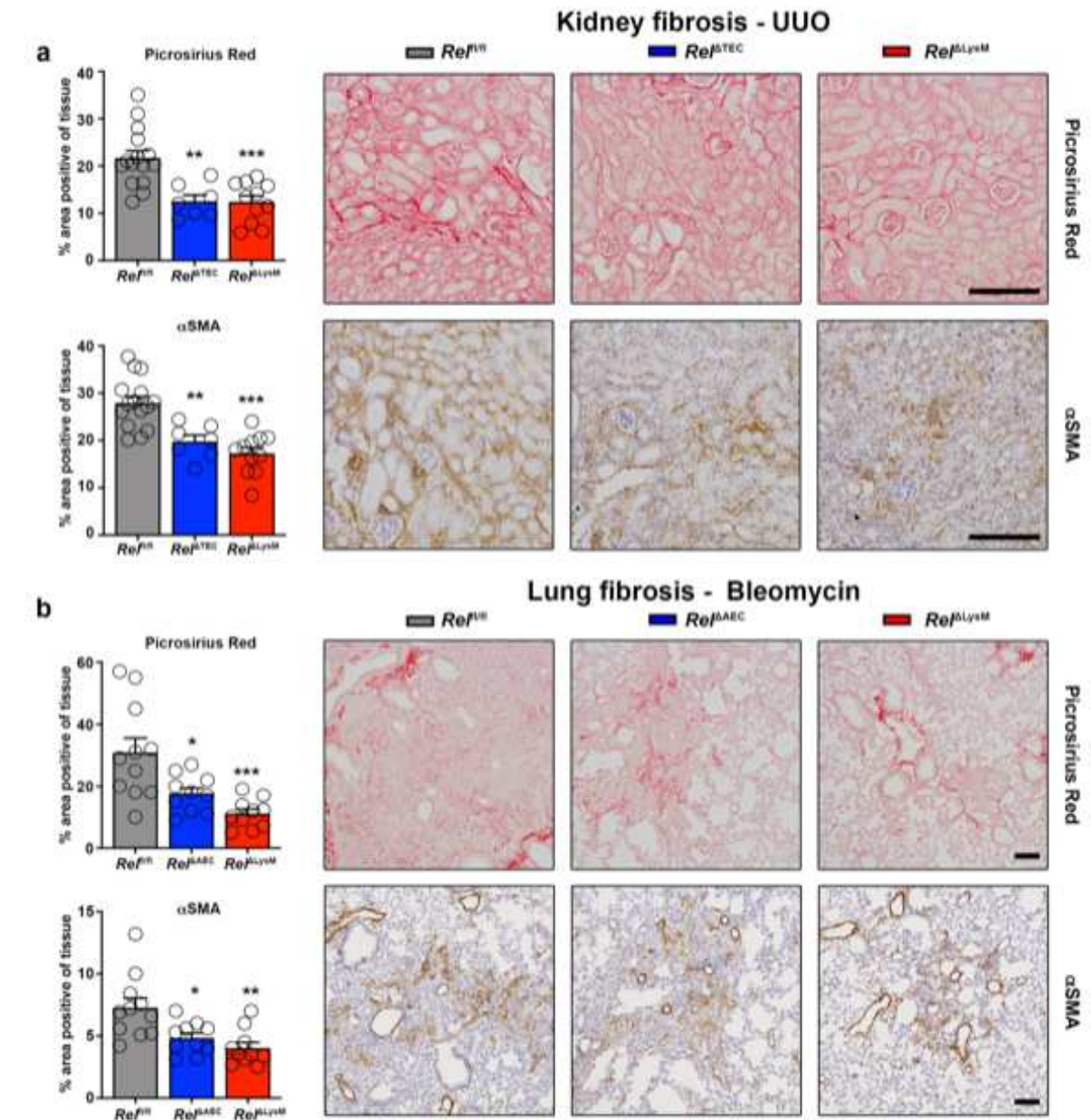


Figure 5. Epithelial or macrophage specific deletion of c-Rel limits renal and pulmonary fibrosis

(a) Histological quantification and representative images of Picrosirius red stained collagen in UUO injured kidneys of *Ref^{fl/fl}*, *Ref^{ΔTEC}* (p value = 0.0013) and *Ref^{ΔLysM}* (p value = 0.0002) mice and αSMA positive myofibroblasts in UUO injured kidneys of *Ref^{fl/fl}*, *Ref^{ΔTEC}* (p value = 0.002) and *Ref^{ΔLysM}* mice (p value = 0.0005). (b) Histological quantification and representative images of Picrosirius red stained bleomycin injured lungs of *Ref^{fl/fl}*, *Ref^{ΔAEC}* (p value = 0.0155) and *Ref^{ΔLysM}* (p value = 0.0004) mice and

α SMA stained bleomycin injured lungs of *Rel^{ffl}*, *Rel ^{Δ AEC}* (p value = 0.0161) and *Rel ^{Δ LysM}* (p value = 0.0013) mice. Data are mean \pm s.e.m. in a minimum of 7 mice/group for the kidney and 10 mice/group for the lung. Scale bars equal 100 microns. All P values were calculated using a one-way ANOVA with Tukey post- hoc t-test. P values equal *P<0.05, **P<0.01 and ***P<0.001.

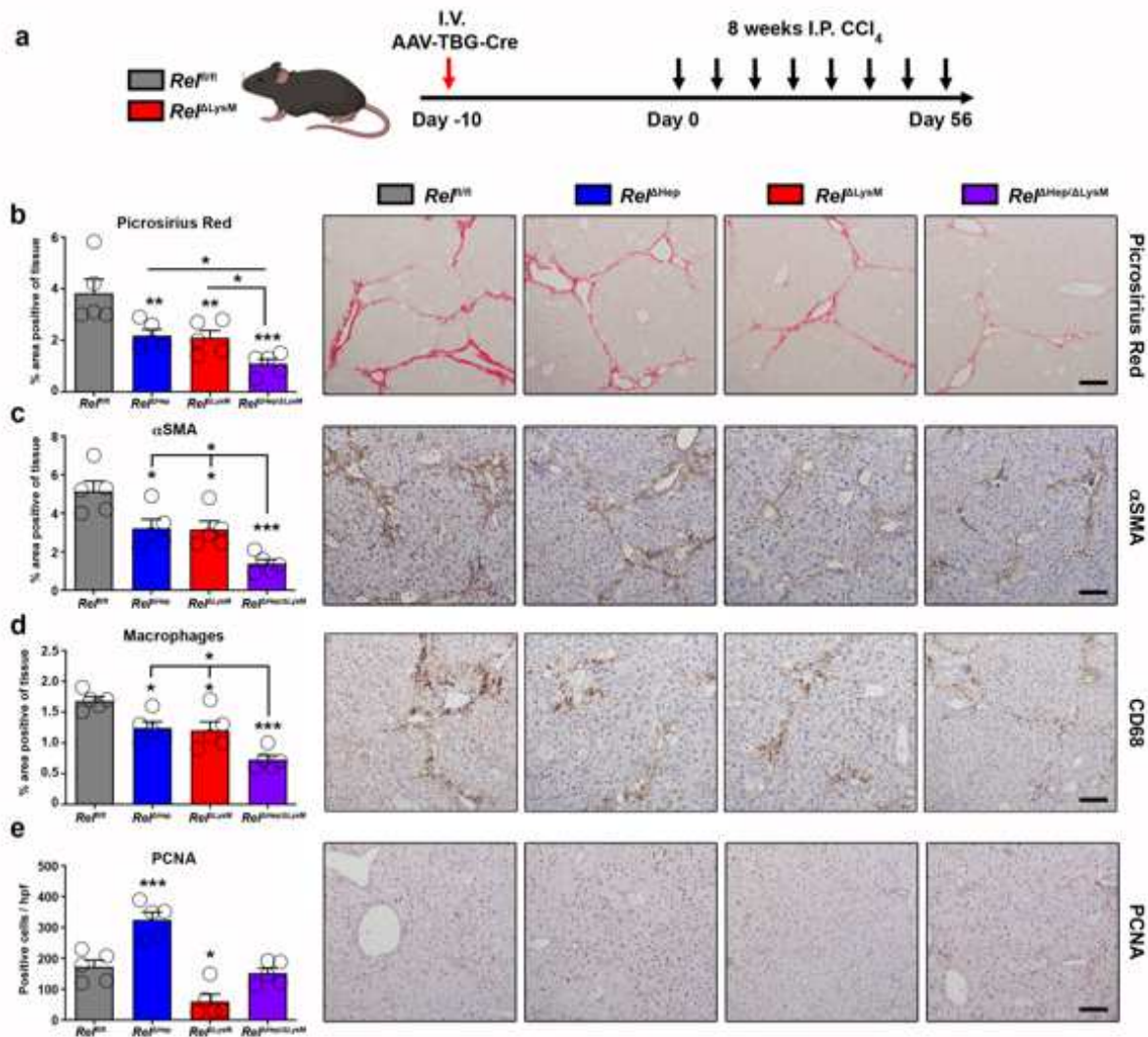


Figure 6. Epithelial and macrophage c-Rel signalling synergistically promote hepatic fibrosis but antagonistically regulate hepatic regeneration in mice

(a) Schematic shows the timeline of intravenous injection administration of adeno-associated virus expressing Cre recombinase (AAV-TBG-Cre) to $ReI^{fl/fl}$ or $ReI^{\Delta LysM}$ mice to create $ReI^{\Delta Hep}$ and $ReI^{\Delta Hep/\Delta LysM}$ prior to chronic CCl_4 injury. (b) Histological quantification and representative images of Picrosirius red stained sections from chronic CCl_4 injured $ReI^{fl/fl}$, $ReI^{\Delta Hep}$ (p value = 0.0093), $ReI^{\Delta LysM}$ (p value = 0.0074) and $ReI^{\Delta Hep/\Delta LysM}$ (p value = 0.0001) mice. (c) Histological quantification and representative images of α SMA stained sections from chronic CCl_4 injured $ReI^{fl/fl}$, $ReI^{\Delta Hep}$ (p value = 0.028), $ReI^{\Delta LysM}$ (p value = 0.023) and $ReI^{\Delta Hep/\Delta LysM}$ (p value = 0.0001) mice. (d)

Histological quantification and representative images of CD68 (macrophages) sections from chronic CCl₄ injured *Rel^{fffl}*, *Rel^{ΔHep}* (p value = 0.0316), *Rel^{ΔLysM}* (p value = 0.0181) and *Rel^{ΔHep/ΔLysM}* (p value = 0.00012) mice. (e) Histological quantification and representative images of PCNA stained sections from chronic CCl₄ injured *Rel^{fffl}*, *Rel^{ΔHep}* (p value = 0.0008), *Rel^{ΔLysM}* (p value = 0.0106) and *Rel^{ΔHep/ΔLysM}* mice. Data are mean ± s.e.m. in 5 mice/group. Scale bars equal 100 microns. All P values were calculated using a one-way ANOVA with Tukey post-hoc t-test (* P <0.05, ** P <0.01, *** P <0.001).

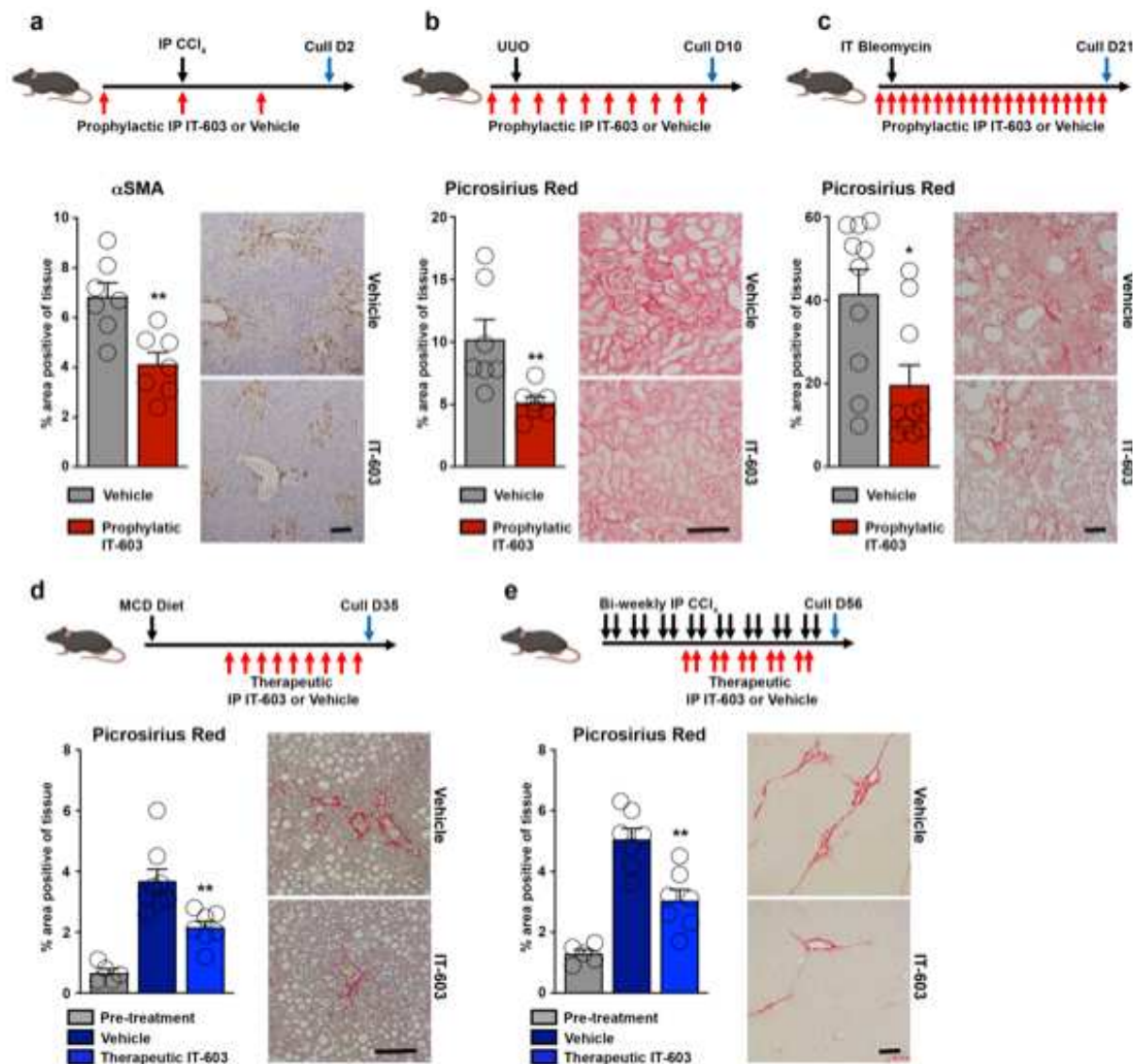


Figure 7: Pharmacological inhibition of c-Rel limits fibrogenesis in murine models of liver, kidney and lung injury

(a-c) Diagrams show experimental timelines of CCl₄, UUO or bleomycin induced liver, kidney or lung fibrosis ± prophylactic IT-603 (c-Rel inhibitor) therapy. Histological quantification and representative images of αSMA stained liver (p value = 0.0031) and Picrosirius red stained kidney (p value = 0.0099) or lungs (p value = 0.01) following their respective injury. Data are mean ± s.e.m. in 7, 7 and 10 mice/group for liver, kidney and lung respectively. (d-e) Diagrams show experimental timelines of methionine choline deficient diet (MCD) fed or chronic CCl₄ induced liver fibrosis ±

therapeutic administration of IT-603. Histological quantification and representative images of Picrosirius red stained MCD (p value = 0.0044) or chronic CCl₄ (p value = 0.001) injured livers pre-treatment and ± therapeutic administration of IT-603. Data are mean ± s.e.m. in 5 pre-treatment mice, 8 vehicle treated MCD mice and 7 IT-603 treated MCD fed mice. Data are mean ± s.e.m. in 5 pre-treatment mice, 7 vehicle treated chronic CCl₄ injured mice and 7 IT-603 treated chronic CCl₄ injured mice. Scale bars equal 100 microns. (a-c) P values calculated using two-sided student T Test. (d-e) P values were calculated using a one-way ANOVA with Tukey post- hoc t-test. P values equal *P<0.05 and **P<0.01 versus vehicle treatment.

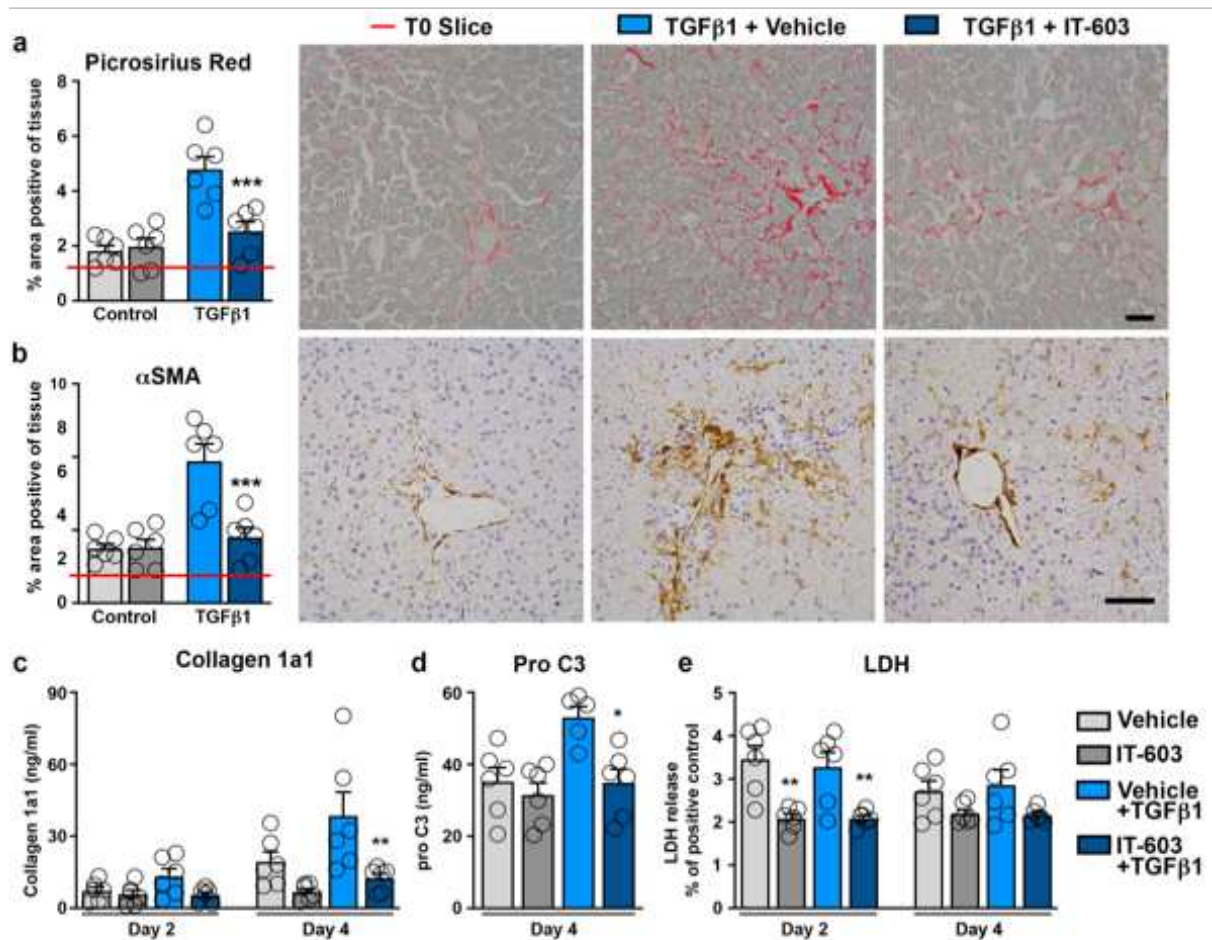
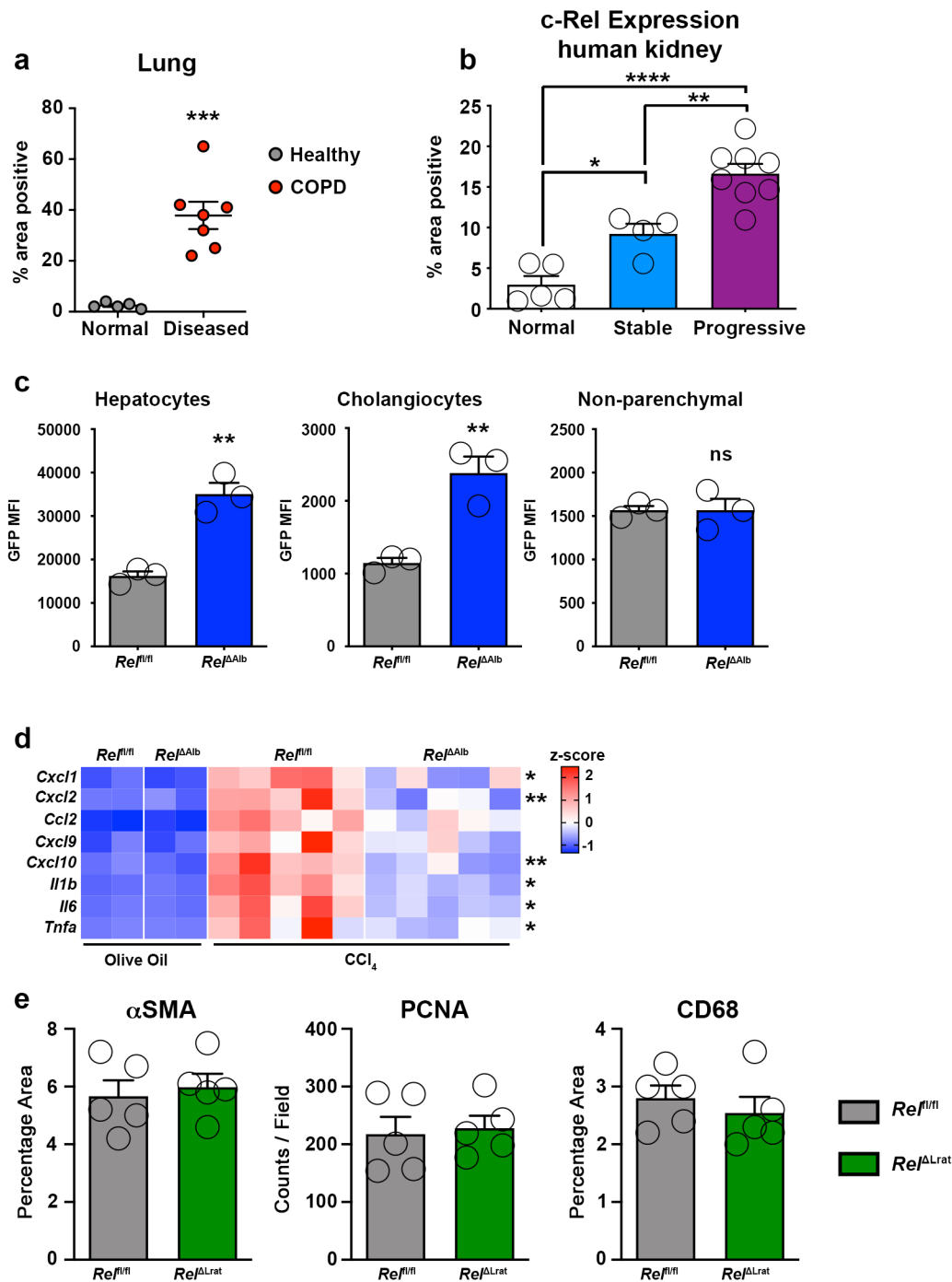


Figure 8: Pharmacological inhibition of c-Rel limits fibrogenesis in human precision cut liver slices

(a-b) Representative images and histological quantification of (a) Picrosirius red (p value = 0.0009) and (b) αSMA (p value = 0.0006) stained liver slices ± TGFβ1 ± IT-603 therapy. Red line denotes the value for the T=0 slice. (c-d) Quantification of (c) soluble collagen (p value = 0.0023) and (d) the neo-epitope pro C3 (p value 0.0286) released from fibrotic liver slices ± IT-603 therapy. (e) Graph showing average LDH release in the media expressed as a percentage (%) of positive control (LDH levels in media from a PCS where maximal death was induced by multiple freeze/thaws – normalized to media volume) where p values = 0.0044 and 0.0004 for IT-603 and IT-603+TGFβ1 respectively. Images are representative of n=3 independent slice experiments. Data are mean ± s.e.m. and representative of slices generated from 3

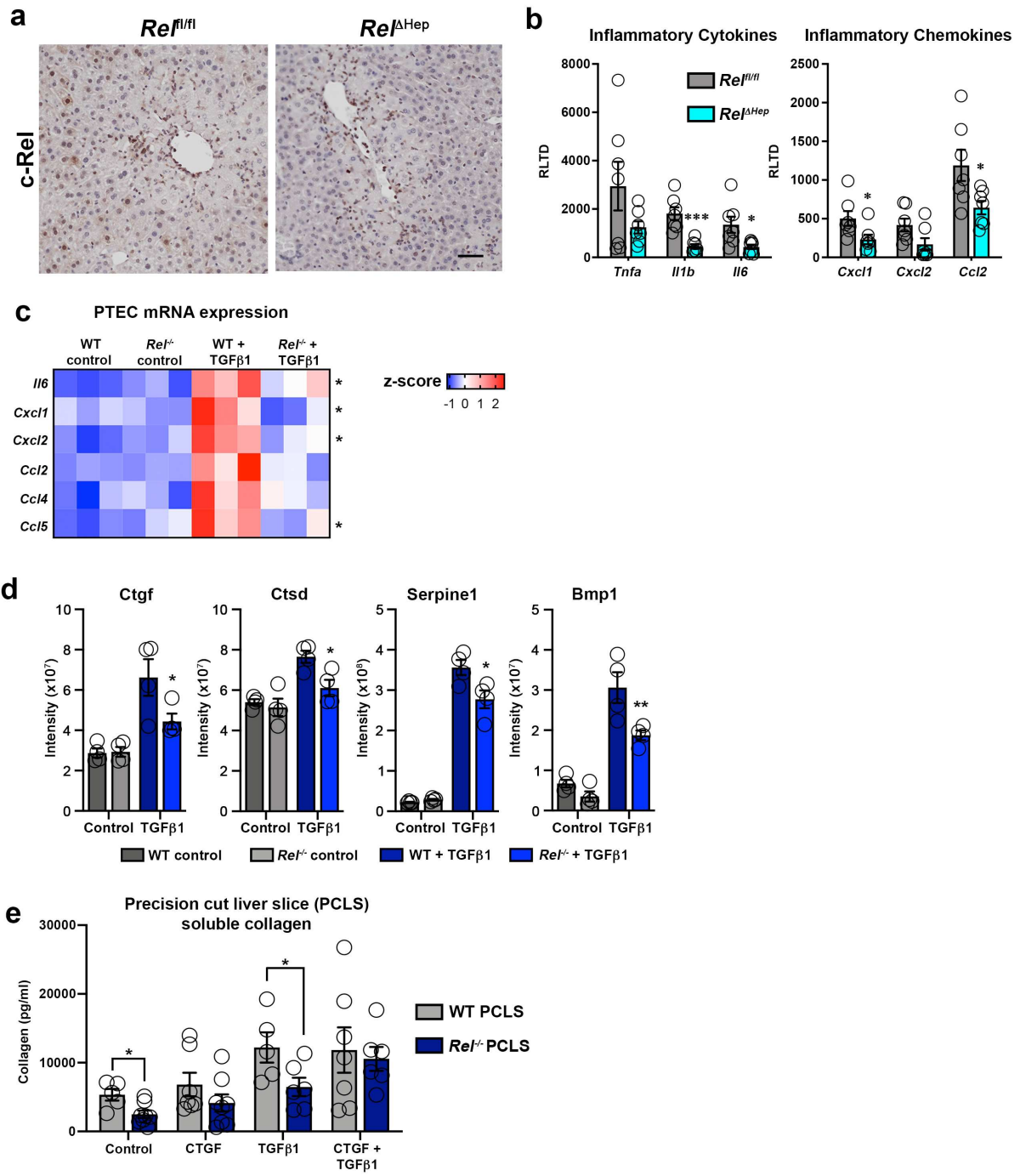
independent donors performed in duplicate. Scale bars equal 100 microns. P values were calculated using two-way ANOVA with Tukey post- hoc t-test (*P<0.05, **P<0.01 and ***P<0.001).



Extended data Fig 1. c-Rel correlates with disease progression in chronic kidney disease and is elevated in chronic lung disease. Investigation of the cell specific actions of c-Rel in preclinical models of liver injury.

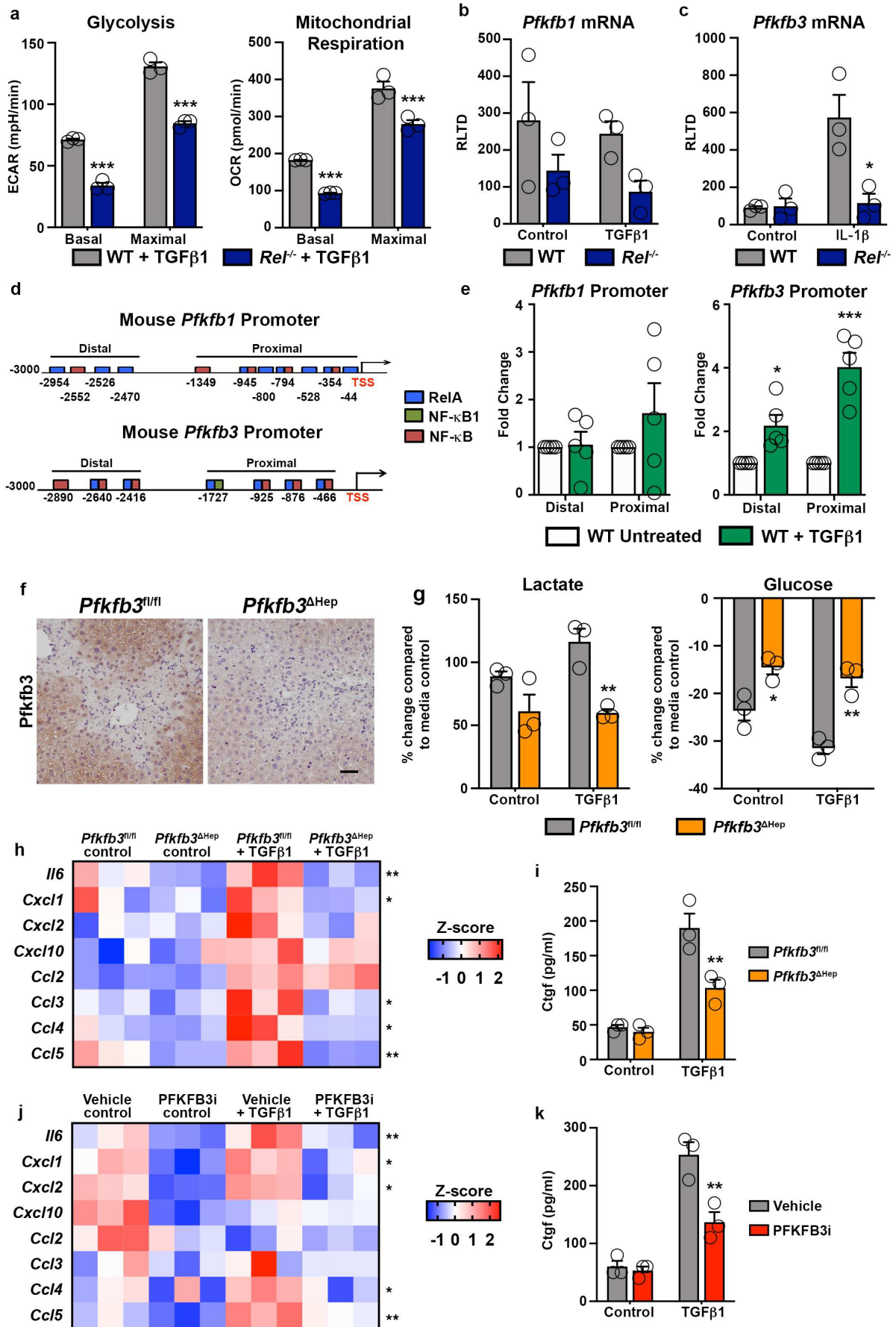
(a) Graph showing average percentage area of c-Rel stained tissue in (n=5) normal lung and (n=7) chronic obstructive pulmonary disorder (COPD) (P value = 0.0003). (b) Graph showing average percentage area of c-Rel stained tissue in (n=5) normal human kidney and patients with stable (n=4, p value = 0.0185) or progressive kidney disease (n=8, p value = 0.003). Normal vs progressive p value <0.0001 (c) Graphs showing the Mean Fluorescence Intensity (MFI) of GFP in hepatocytes (p value = 0.0026), Cholangiocytes (EPCAM+, p value = 0.0026) and non-parenchymal (EPCAM-) cells from the livers of *Rel^{fl/fl}* and *Rel^{ΔAlb}* mice. Data are mean ± s.e.m of 3 mice/group. (d) Heatmap showing gene expression of *Cxcl1*, *Cxcl2*, *Ccl2*, *Cxcl9*, *Cxcl10*, *Il1b*, *Il6* and *Tnfa* in olive oil vehicle control and acute CCl_4 injured *Rel^{fl/fl}* and *Rel^{ΔAlb}*

mice. Asterisk denotes significance between CCl₄ injured *Rel^{fl/fl}* and *Rel^{ΔAlb}* mice; there is no significant difference between olive oil treated groups. (e) Histological assessment of αSMA, PCNA and CD68 stained liver sections in acute CCl₄ injured *Rel^{fl/fl}* and *Rel^{ΔLrat}* mice. Data in graphs are mean ± s.e.m of n=5. (a, c, e) P values were calculated using unpaired two-sided T test. (b) P value was calculated using a one-way ANOVA with Tukey post-hoc t-test (* P <0.05, ** P <0.01, *** P <0.001 and **** P <0.0001).



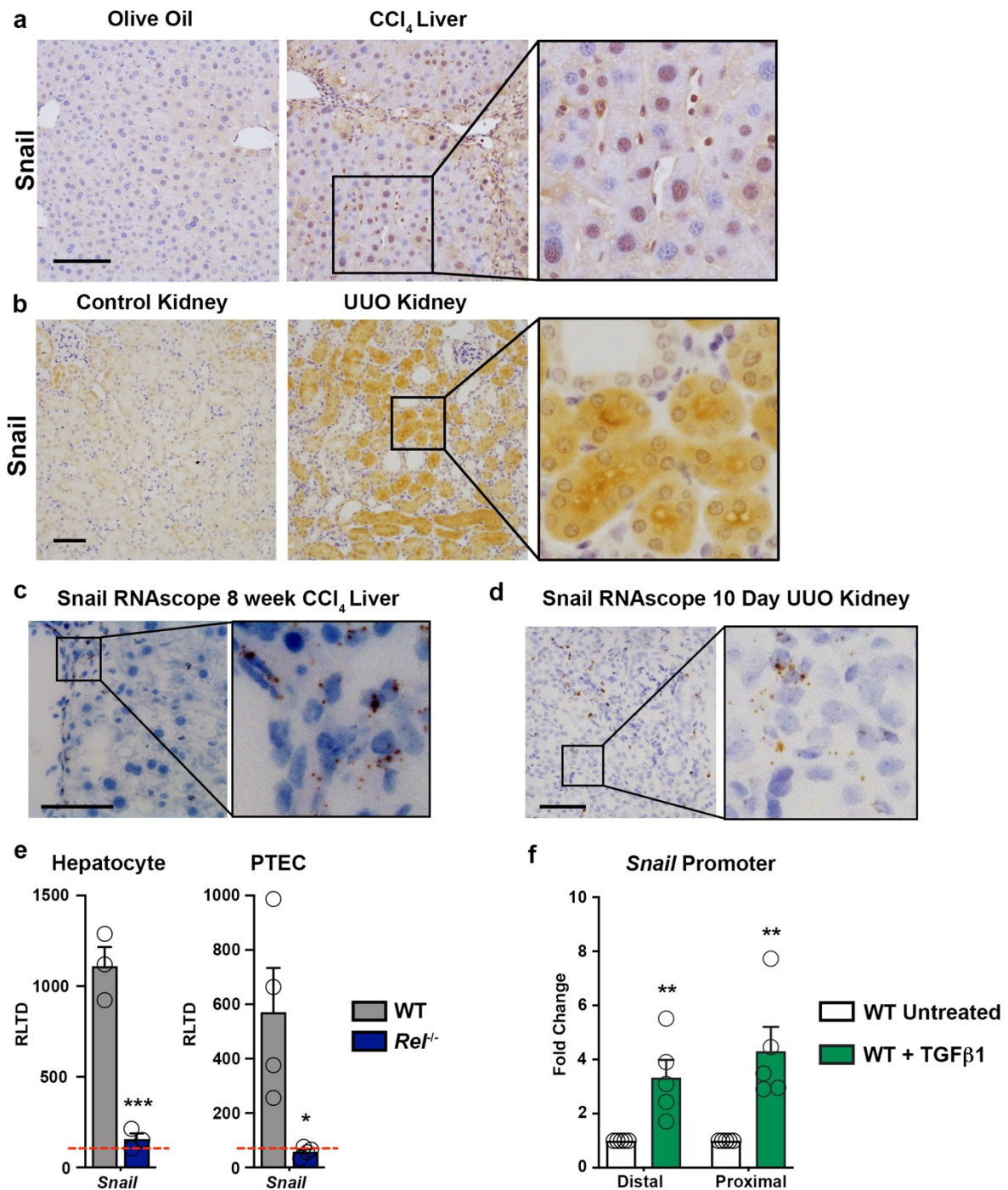
Extended data Fig 2. c-Rel regulates epithelial dedifferentiation and fibrogenic gene expression. (a) Representative images of c-Rel staining in CCl_4 injured $\text{Rel}^{\text{fl/fl}}$ and $\text{Rel}^{\Delta\text{Hep}}$ mice. Representative of $n=7$ mice/group. Scale bar represents $100\mu\text{m}$. (b) Graph shows mRNA levels of inflammatory cytokines *Tnfa*, *Il1b* ($p=0.00038$) and *Il6* (p value = 0.022) and the inflammatory chemokines *Cxcl1* (p value = 0.0034), *Cxcl2* ($p=0.054$) and *Ccl2* ($p=0.0029$), in CCl_4 injured livers of $\text{Rel}^{\text{fl/fl}}$ and $\text{Rel}^{\Delta\text{Hep}}$ mice. Data are mean \pm s.e.m of 7 mice/group. (c) Heatmap showing relative mRNA expression of *Il-6*, *Cxcl1*, *Cxcl2*, *Ccl2*, *Ccl4* and *Ccl5* in WT and $\text{Rel}^{-/-}$ proximal tubular epithelial cells (PTEC) stimulated with or without TGF β 1. (d) Graphs show relative levels of *Ctgf* (p value = 0.034), *Ctsd* ($p= 0.039$), *Serpine1* ($p=0.04$) and *Bmp1* ($p=0.0054$) protein expressed as Intensity in control and TGF β 1 treated WT and $\text{Rel}^{-/-}$ hepatocytes. Data are from 4 independent cell isolations/group. (e)

Quantification of soluble collagen (pg/ml) released from precision cut liver slices (PCLS) generated from WT and *Rel^{-/-}* liver, stimulated \pm TGF β 1 \pm CTGF where (control p value = 0.012 and TGF β 1 p value = 0.045). Data are from PCLS generated 3 different donors/genotype. (b,d) P values were calculated using unpaired two-sided t-test. (d) P values were calculated using the R package LIMMA (* P <0.05, ** P <0.01 and ***P<0.001).



Extended data Fig 3: c-Rel regulates metabolic enzymes to induce epithelial

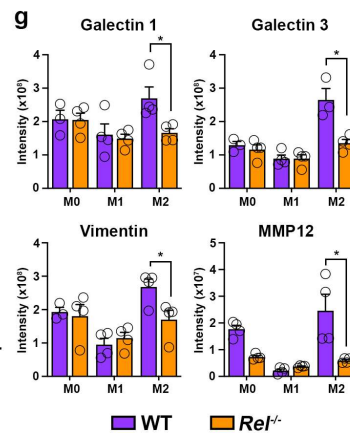
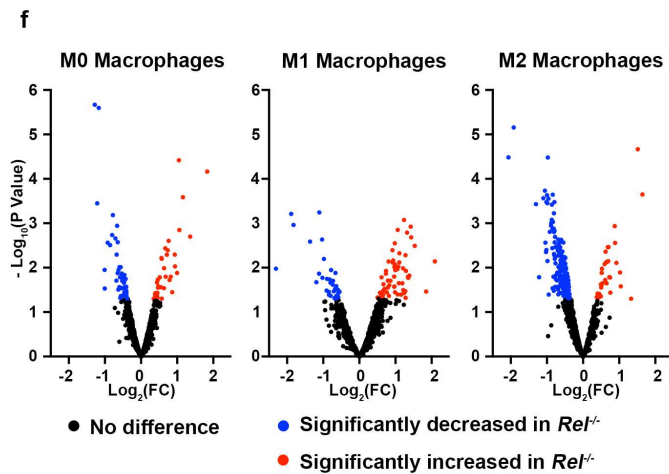
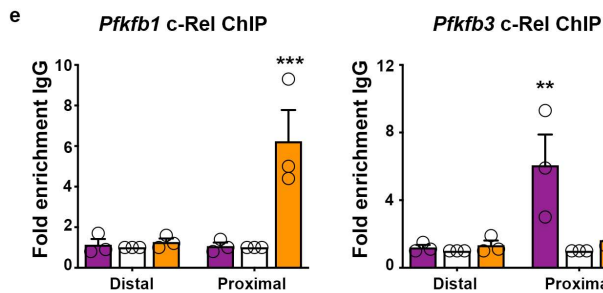
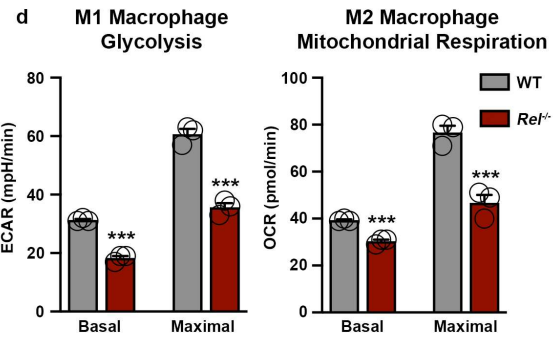
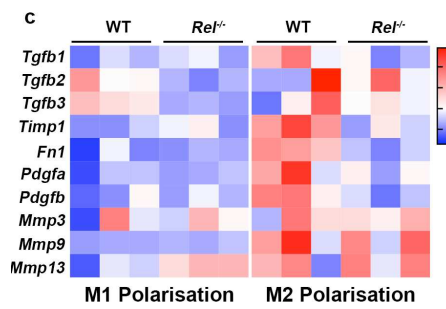
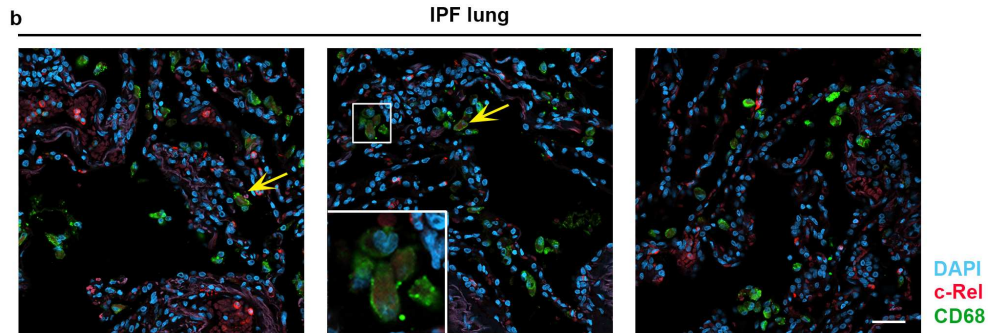
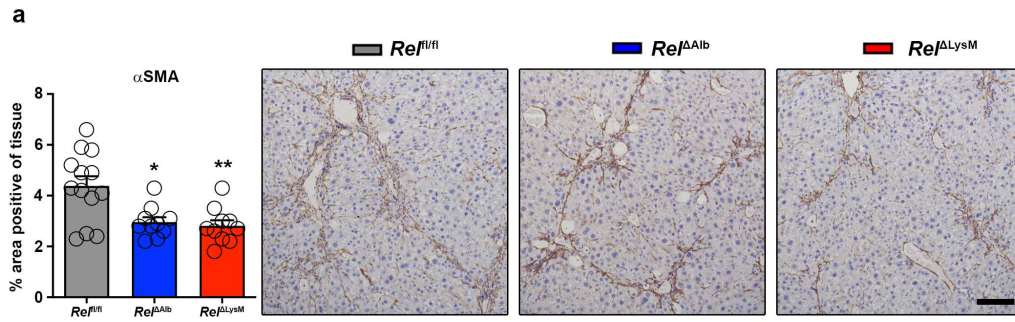
dedifferentiation and fibrogenic gene expression. (a) Seahorse analysis of basal ($p < 0.0001$) and maximal ($p < 0.0001$) glycolysis (extracellular acidification rate, ECAR) and basal ($p < 0.0007$) and maximal ($p < 0.0004$) mitochondrial respiration (oxygen consumption rate, OCR) in WT and *Rel*^{-/-} hepatocytes stimulated \pm TGF β 1. (b) Graph shows mRNA expression of *Pfkfb1* in WT and *Rel*^{-/-} hepatocytes stimulated \pm TGF β 1. (c) Graph shows mRNA expression of *Pfkfb3* in WT and *Rel*^{-/-} hepatocytes stimulated \pm IL-1 β . (p value=0.025) (d) Schematic representation of RelA, NF- κ B1 and NF- κ B binding sites in the murine *Pfkfb1* and *Pfkfb3* promoters. (e) ChIP analysis of c-Rel at the proximal and distal regions of the *Pfkfb1* promoter and the proximal ($p < 0.0001$) and distal ($p = 0.0185$) regions of the *Pfkfb3* promoter in WT hepatocytes treated \pm TGF β 1. (f) Representative images show PFKFB3 immunohistochemical staining in liver sections from acute CCl₄ injured *Pfkfb3*^{fl/fl} and *Pfkfb3* ^{Δ hep} mice. Images are representative of $n = 5$ mice/group. Scale bar is 100 μ m. (g) Graphs show media lactate in control and TGF β 1 ($p = 0.0064$) stimulated and glucose levels in control ($p = 0.0227$) and TGF β 1 ($p = 0.00284$) stimulated in hepatocytes isolated from *Pfkfb3*^{fl/fl} and *Pfkfb3* ^{Δ hep} mice and stimulated \pm TGF β 1. (h) Heatmap showing secreted *Il-6*, *Cxcl1*, *Cxcl2*, *Cxcl10*, *Ccl2*, *Ccl3*, *Ccl4* and *Ccl5*, measured by MSD in the media of hepatocytes isolated from *Pfkfb3*^{fl/fl} and *Pfkfb3* ^{Δ hep} mice and stimulated \pm TGF β 1. (i) Quantification of connective tissue growth factor (CTGF) in pg/ml in the culture media of hepatocytes isolated from *Pfkfb3*^{fl/fl} and *Pfkfb3* ^{Δ hep} mice and stimulated \pm TGF β 1 ($p = 0.0027$) (j) Heatmap showing secreted *Il-6*, *Cxcl1*, *Cxcl2*, *Cxcl10*, *Ccl2*, *Ccl3*, *Ccl4* and *Ccl5*, measured by MSD in the media of WT hepatocytes stimulated \pm TGF β 1 \pm the Pfkfb3 inhibitor 3PO. (k) Quantification of connective tissue growth factor (CTGF) in pg/ml in the culture media of WT hepatocytes stimulated \pm TGF β 1 \pm the Pfkfb3 inhibitor 3PO ($p = 0.0013$). Data in graphs are mean \pm s.e.m. in $n = 3$ (g,i,k), $n = 4$ (a,b,c) or $n = 5$ (e) independent cell isolations/condition. All p values were calculated using a two-way ANOVA with Tukey post-hoc t-test (* $P < 0.05$, ** $P < 0.01$ and *** $P < 0.001$).



Extended data Fig 4: c-Rel dependent Snail regulation in chronic liver and kidney disease

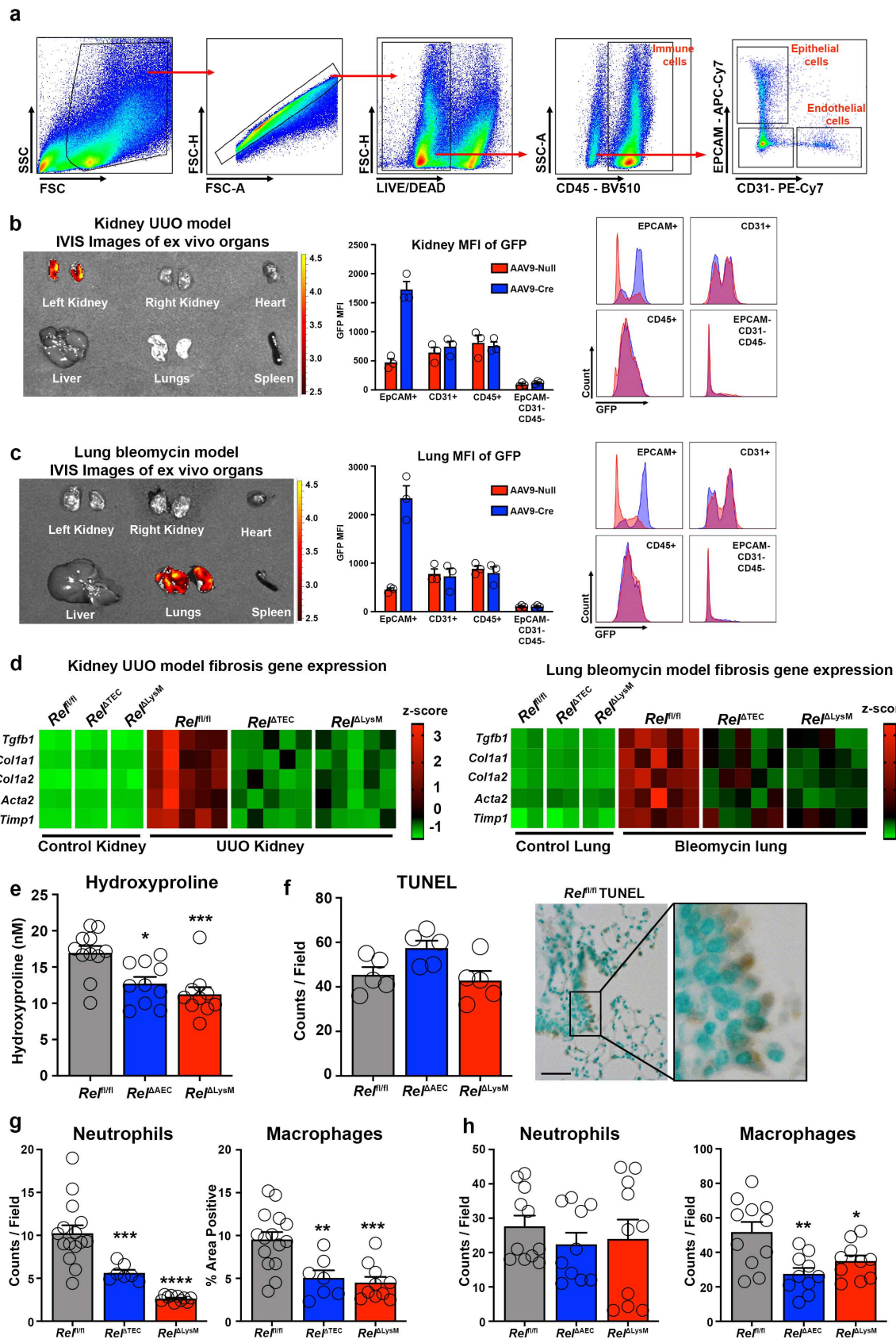
(a) Representative images show expression of Snail in normal and chronic CCl₄ injured liver. (b) Representative images show Snail in normal and UUO injured kidney. (c) Representative images of Snail transcript in epithelial cells detected by RNAScope in fibrotic chronic CCl₄ injured fibrotic mouse liver. (d) Representative images of *Snail* transcript in epithelial cells detected by RNAScope in fibrotic UUO mouse kidney. All representative images are representative of n=5 mice/group. (a-b) Scale bars equal 100 microns (c-d) Scale bars equal 50 microns. (e) Graph showing mRNA levels of *Snail* in TGFβ1 treated hepatocytes (p=0.0001) and proximal tubular epithelial cells (PTEC) (p=0.02) isolated from WT and *Rel*^{-/-} mice. Data in graphs are mean ± s.e.m. in n=3 independent cell isolations. (f) Graph showing

ChIP analysis of c-Rel binding to distal ($p=0.0074$) and proximal ($p=0.0063$) regions of the *Snail* promoter in WT hepatocytes stimulated \pm TGF β 1. Data in graphs are mean \pm s.e.m. in $n=5$ independent cell isolations. P values were calculated using unpaired two-sided t-test (e) and a ratio paired t-test (f) (* P <0.05, ** P <0.01 and *** P <0.001).



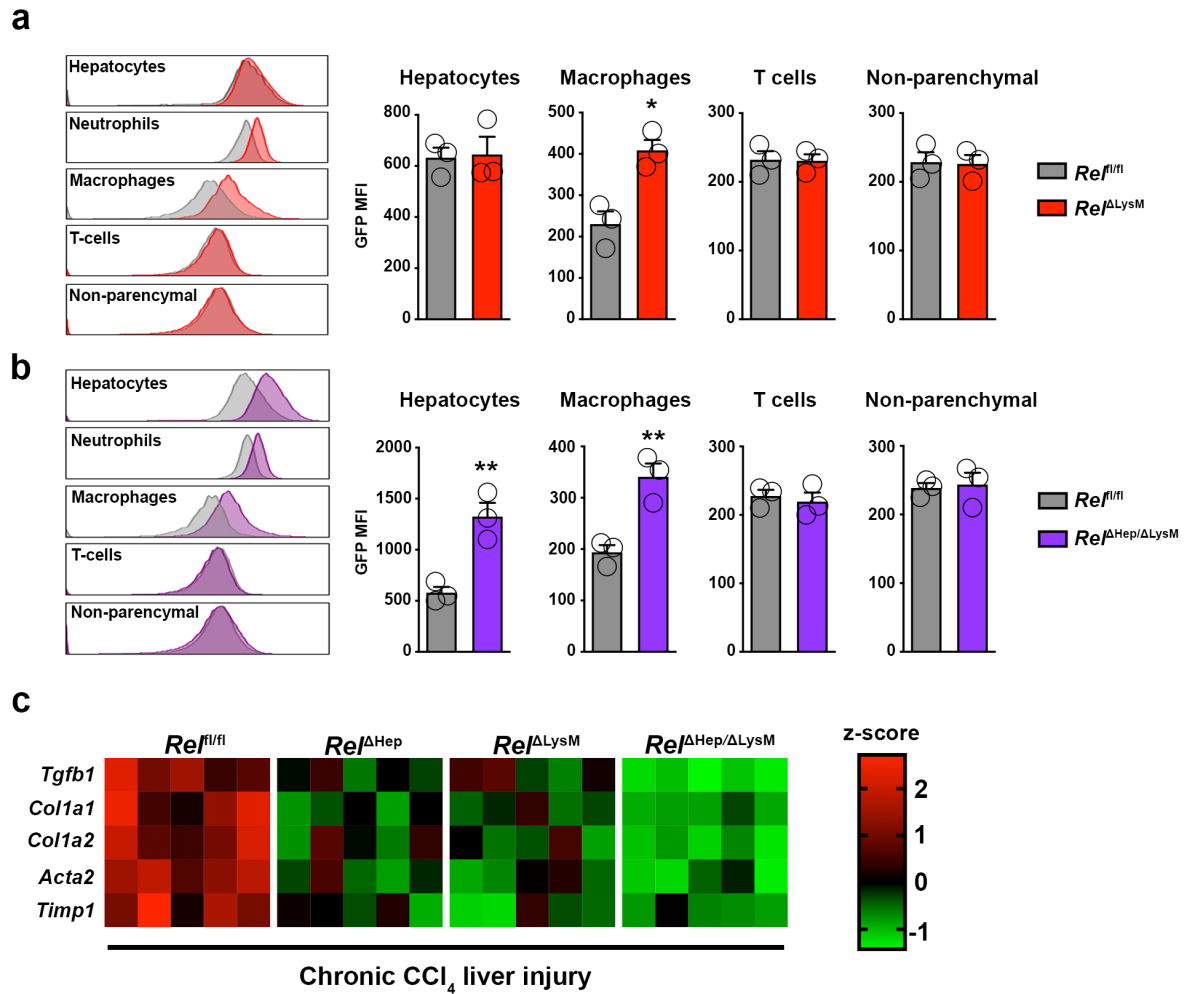
Extended data Fig 5: c-Rel regulates macrophage polarisation to drive tissue fibrosis.

(a) Histological assessment and representative images of α SMA stained liver sections in acute CCl_4 injured in (n=13) $Rel^{fl/fl}$, (n=7) $Rel^{\Delta Alb}$ (p=0.0116), and (n=10) $Rel^{\Delta LysM}$ (p=0.0051) mice. Data are mean \pm s.e.m. Scale bar equals 100 microns. P values were calculated using a one-way ANOVA with Tukey post- hoc t-test. (b) Representative low power immuno-fluorescence images show c-Rel (red), CD68 (green) and nuclear (blue) staining in diagnosed idiopathic pulmonary fibrosis lung sections. Yellow arrows denote co-localisation of c-Rel and CD68. Scale bar equals 50 microns. Images are representative of n=8 IPF stained sections. (c) Heat map showing relative mRNA expression of fibrogenic markers; *Tgfb1*, *Tgfb2*, *Tgfb3*, *TIMP1*, *Fn1*, *Pdgfa*, *Pdgfb*, *Mmp3*, *Mmp9* and *Mmp13* in M1 and M2 polarised WT and $Rel^{-/-}$ BMDMs. (d) Graphs show, seahorse analysis of basal (p<0.0001) and maximal (p=0.0004) glycolysis (extracellular acidification rate, ECAR) and basal (p=0.0002) and maximal (p=0.0024) mitochondrial respiration (oxygen consumption rate, OCR) in M1 and M2 polarised WT and $Rel^{-/-}$ BMDMs. Data are mean \pm s.e.m. from 3 independent cell isolations/group. (e) ChIP analysis of c-Rel binding to distal and proximal (p=0.004) regions of the *Pfkfb3* promoter and to distal and proximal (p=0.003) regions of the *Pfkfb1* promoters in WT BMDM in response to M1 and M2 polarisation. Data are mean \pm s.e.m. from 3 independent cell isolations/group. (d-e) P values were calculated using two-way ANOVA with Tukey post-hoc t-test. Denoted significance refers to comparisons between WT and $Rel^{-/-}$ macrophages polarised to either an M1 or M2 phenotype. (f) Volcano plots show differentially expressed proteins detected by proteomic analysis of the secretome of M0, M1 and M2 polarised WT and $Rel^{-/-}$ BMDMs. (g) Graphs show relative levels of Galectin 1 (p=0.0031), Galectin 3 (p=0.0013), Vimentin (p=0.0128) and Matrix Metalloproteinase 12 (MMP12) (p<0.0001) expressed as Intensity $\times 10^8$ in M0, M1 and M2 polarised WT and $Rel^{-/-}$ BMDMs. Data are mean \pm s.e.m. from 4 independent cell isolations/group generated 4 different donors/genotype. P values were calculated using the R package LIMMA (* P <0.05, ** P <0.01 and *** P <0.001).



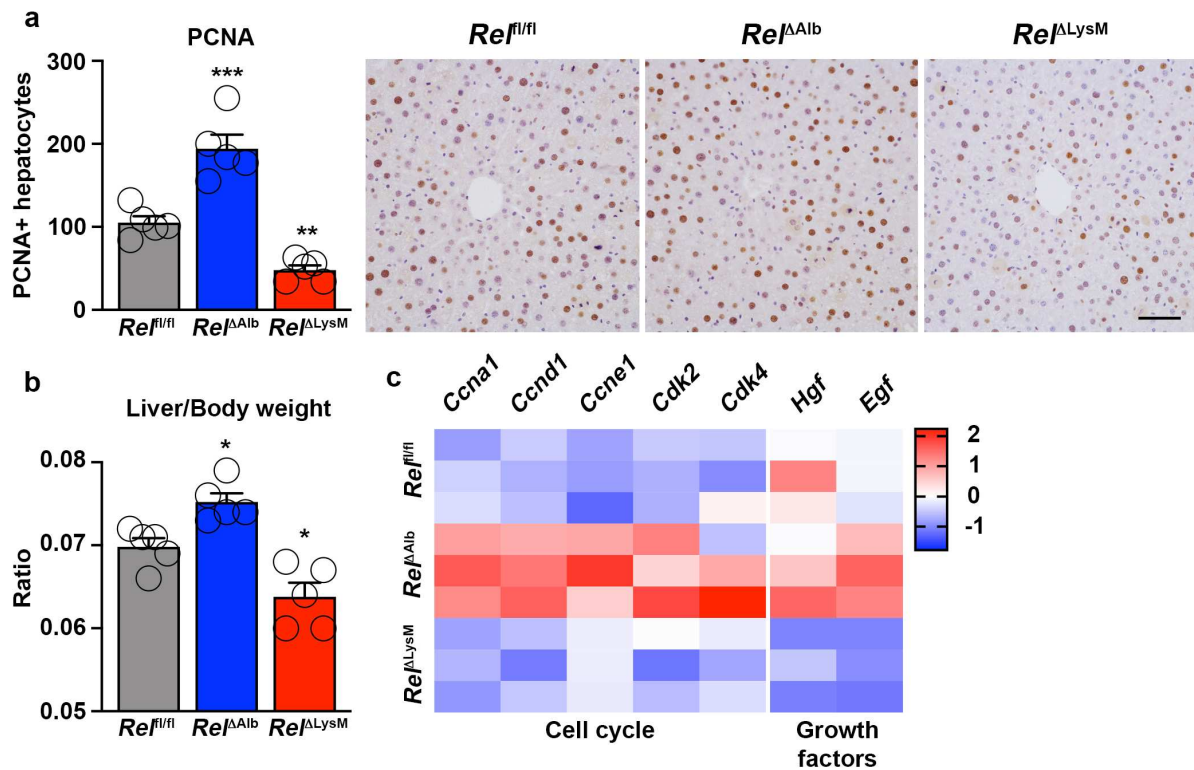
Extended data Fig 6: Validation of epithelial specific deletion of c-Rel in kidney and lung fibrosis models.

(a) Flow cytometry gating strategy to identify immune cells (CD45+), epithelial cells (EPCAM+) and endothelial cells (CD31+) isolated from the kidney or lungs of $Rel^{fl/fl}$, $Rel^{\Delta TEC}$ or $Rel^{\Delta AEC}$ mice respectively. (b-c) *Ex vivo* images of GFP fluorescence signal in the left and right kidneys, heart, liver, lungs and spleen of $Rel^{\Delta TEC}$ mice (b) or $Rel^{\Delta AEC}$ mice (c) imaged using an In Vivo Imaging System (IVIS). Graph and flow cytometry histograms show the Mean Fluorescence Intensity (MFI) of GFP in EpCAM+, CD31+, CD45+ and EpCAM-CD31-CD45- cells from the kidney of $Rel^{\Delta TEC}$ and $Rel^{fl/fl}$ control mice (b) or from the lung of $Rel^{\Delta AEC}$ and $Rel^{fl/fl}$ control mice (c), n=5 mice/group. (d) Heatmap showing mRNA levels of *Tgfb1*, *Col1a1*, *Col1a2*, *Acta2* and *Timp1* in control versus UUO kidney of $Rel^{fl/fl}$, $Rel^{\Delta TEC}$ and $Rel^{\Delta LysM}$ mice (left) or control versus bleomycin lung of $Rel^{fl/fl}$, $Rel^{\Delta AEC}$ and $Rel^{\Delta LysM}$ mice (right). Heatmap data are from 2 mice/group in control kidney or lung and 5 mice/group in the injured kidney or lung. (e) Quantification of hydroxyproline levels in nM per left lobe of lung tissue from bleomycin injured in $Rel^{fl/fl}$, $Rel^{\Delta AEC}$ (p=0.0105), and $Rel^{\Delta LysM}$ (p=0.0006) mice. (f) Histological assessment and representative images of TUNEL stained lung sections in day 3 bleomycin injured in $Rel^{fl/fl}$, $Rel^{\Delta AEC}$, and $Rel^{\Delta LysM}$ mice. Scale bar is 50 microns. Data are mean \pm s.e.m. in n=5 mice/group. (g) Quantification of neutrophil numbers in UUO injured kidneys of $Rel^{fl/fl}$, $Rel^{\Delta TEC}$ (p=0.0014) and $Rel^{\Delta LysM}$ (p<0.0001) mice and macrophage numbers in UUO injured kidneys of $Rel^{fl/fl}$, $Rel^{\Delta TEC}$ (p=0.0045) and $Rel^{\Delta LysM}$ (p=0.0004) mice. (h) Quantification of neutrophil numbers in Bleomycin injured lungs of $Rel^{fl/fl}$, $Rel^{\Delta AEC}$ and $Rel^{\Delta LysM}$ mice and macrophage numbers in Bleomycin injured lungs of $Rel^{fl/fl}$, $Rel^{\Delta AEC}$ (p=0.0018) and $Rel^{\Delta LysM}$ (p=0.0327) mice. (e,g,h) Data are mean \pm s.e.m. in a minimum of 7 mice/group for the kidney and 10 mice/group for the lung. P values were calculated using one-way ANOVA with Tukey post-hoc t-test (* P <0.05, **P <0.01 and ***P <0.001).



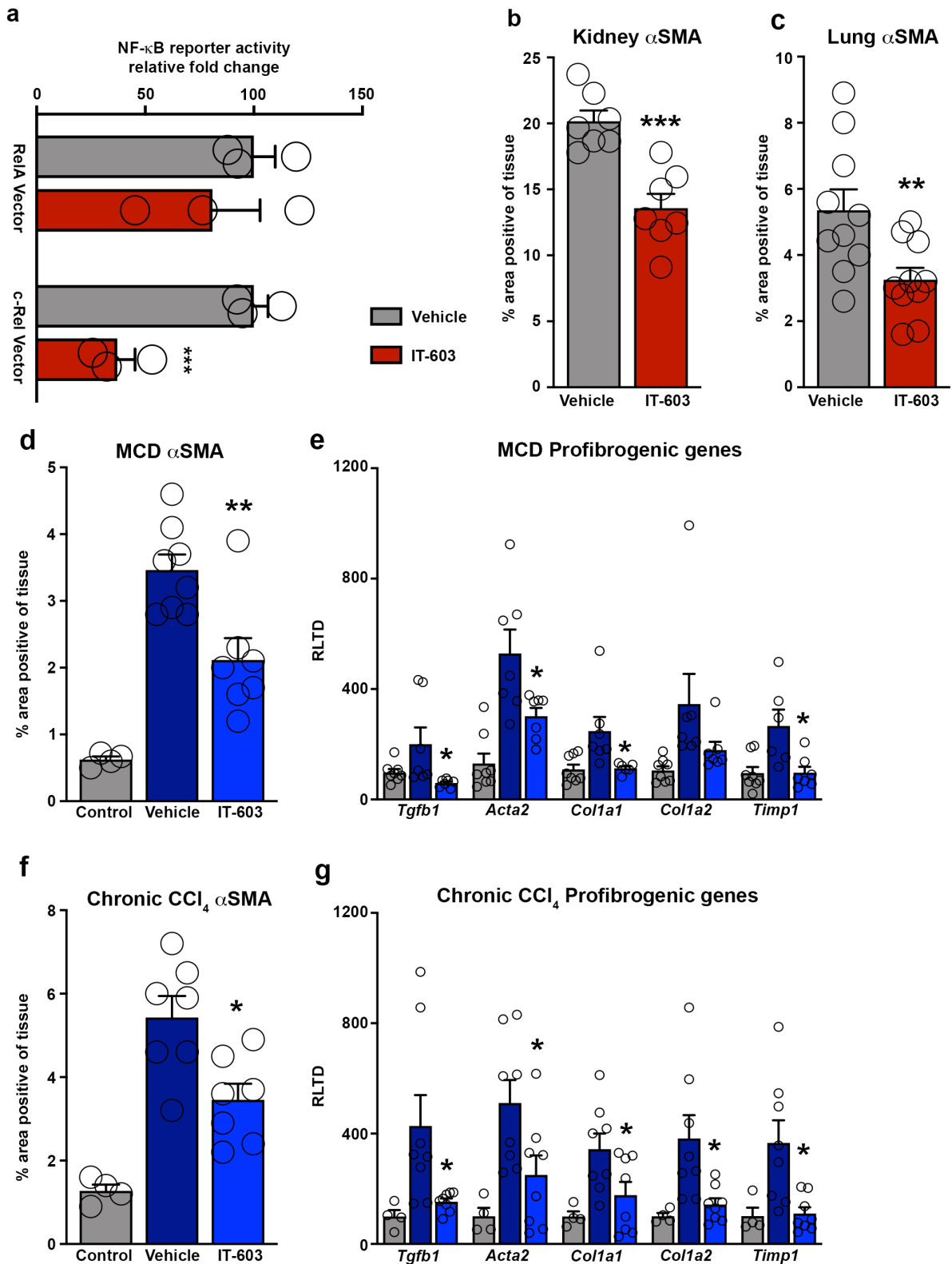
Extended data Fig 7: Validation of single myeloid or dual hepatocyte- and myeloid- specific deletion of c-Rel in mice and analysis of fibrogenic gene expression in these mice during chronic liver injury.

(a) FACS plot and graphs show the Mean Fluorescence Intensity (MFI) of GFP expression in hepatocytes, macrophages (CD45+F4/80+CD11b+) ($p=0.011$), T-cells (CD45+CD3+) and non-parenchymal cells (CD45-) from the liver of *ReI^{fl/fl}* versus *ReI^{ΔLysM}* mice, $n=3$ mice/group. (b) FACS plot and graphs show the Mean Fluorescence Intensity (MFI) of GFP expression in hepatocytes ($p=0.007$), macrophages (CD45+F4/80+CD11b+) ($p=0.007$), T-cells (CD45+CD3+) and non-parenchymal cells (CD45-) from the liver of *ReI^{fl/fl}* versus *ReI^{ΔHep/ΔLysM}* mice, $n=3$ mice/group. (c) Heatmap showing mRNA levels of *Tgfb1*, *Col1a1*, *Col1a2*, *Acta2* and *Timp1* in the CCl₄ injured liver of *ReI^{fl/fl}*, *ReI^{ΔHep}*, *ReI^{ΔLysM}* and *ReI^{ΔHep/ΔLysM}* mice. P values were calculated using two-sided t-test (* $P < 0.05$)



Extended data Fig 8: c-Rel signaling in hepatocyte and macrophages differentially regulate liver regeneration via regulation of cell cycle genes and mitogenic factors.

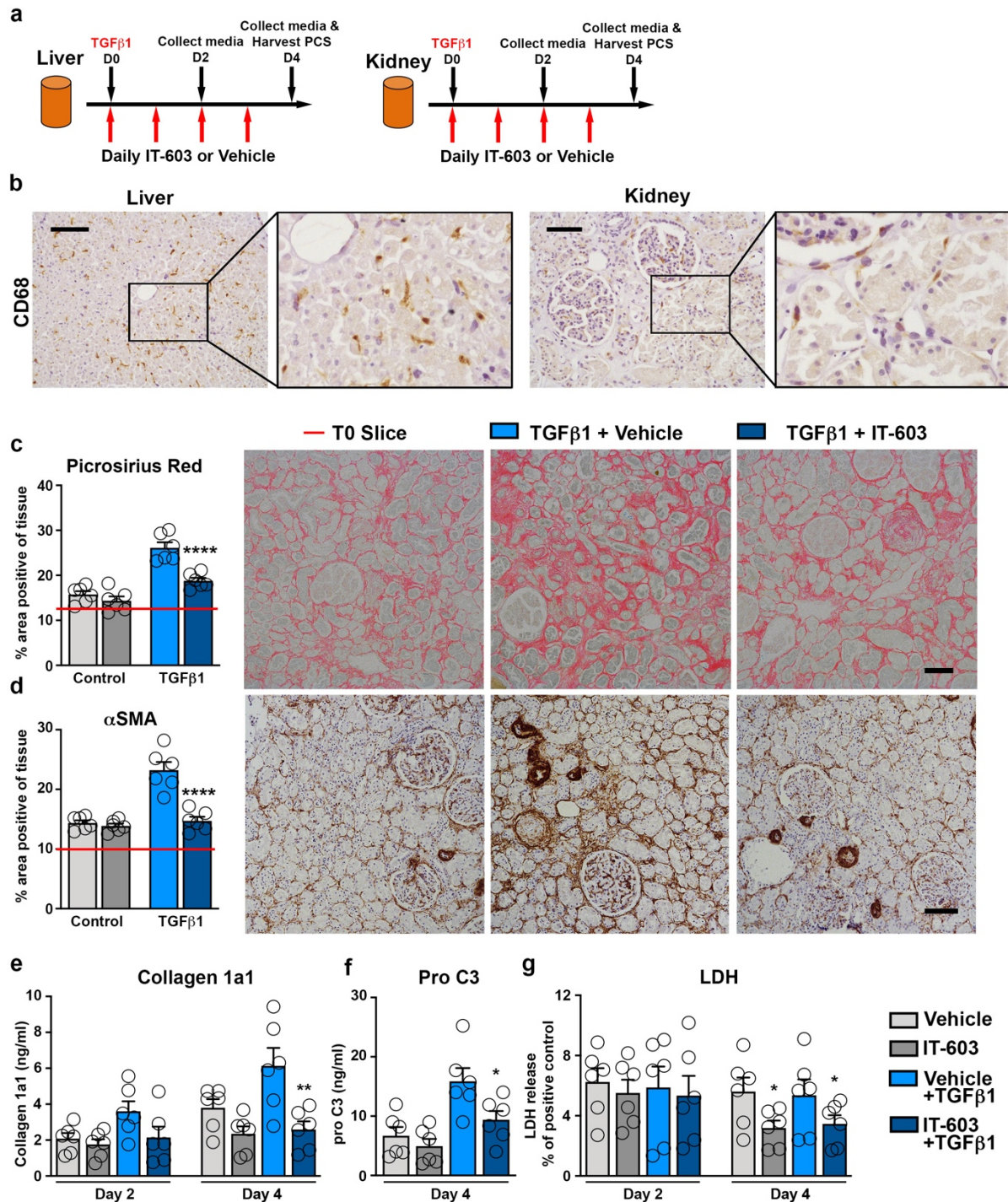
(a) Histological assessment and representative images of PCNA positive hepatocytes in 48h partial hepatectomy injured *Rel^{fl/fl}*, *Rel^{ΔAlb}* ($p=0.0003$) and *Rel^{ΔLysM}* ($p=0.0096$) mice. Scale bar is 100 microns. (b) Graph shows average liver/body weight ratio 48h post partial hepatectomy in *Rel^{fl/fl}*, *Rel^{ΔAlb}* ($p=0.0318$) and *Rel^{ΔLysM}* ($p=0.0178$) mice. (c) Heat map showing relative hepatic mRNA expression of cell cycle genes; *Ccna1*, *Ccnd1*, *Ccne1*, *Cdk2*, *Cdk4* and mitogenic proteins; *Hgf* and *Egf* at 48h post partial hepatectomy in *Rel^{fl/fl}*, *Rel^{ΔAlb}* and *Rel^{ΔLysM}* mice. Data are mean \pm s.e.m. in $n=5$ mice/group. P values were calculated using one-way ANOVA with Tukey post-hoc t- test (* $P < 0.05$ and ** $P < 0.01$).



Extended data Fig 9: IT-603 attenuates fibrogenesis in murine models of fibrosis.

(a) U937 cells stably expressing 3xNF- κ B-Luc reporter were transiently transfected with RelA or c-Rel expression plasmids. Graph shows RelA and c-Rel induced NF- κ B luciferase reporter activity \pm IT-603 therapy. Data are mean \pm s.e.m. P value = 0.0039. P value was calculated

using an unpaired two-sided t-test (**P<0.001) of 3 independent experiments. (b-c) Histological quantification of α SMA stained kidney (p=0.0004) or lungs (p=0.009) following their respective injury. Data are mean \pm s.e.m. in 7 and 10 mice/group for kidney and lung respectively. P values were calculated using an unpaired two-sided t-test. (d) Histological quantification of α SMA stained chronic MCD diet injured livers at 2 weeks (pre-treatment) and 5 weeks \pm therapeutic administration of IT-603 (p=0.0044). (e) Graphs showing relative hepatic expression of the fibrogenic genes; *Tgfb1* (p=0.039), *Acta2* (p=0.028), *Col1a1* (p=0.036), *Col1a2*, and *Timp1*(p=0.015) in 2-week (pre-treatment) and 5-week methionine choline deficient diet (MCD) fed mice \pm therapeutic administration of IT-603. Data are mean \pm s.e.m. in n=4 control mice 8 vehicle and n=7 IT-603 treated mice/group. (f) Histological quantification of α SMA stained chronic CCl₄ injured livers at 3 weeks (pre-treatment) or 8 weeks \pm therapeutic administration of IT-603 (p=0.0105). (g) Graphs showing relative hepatic expression of the fibrogenic genes; *Tgfb1* (p=0.029), *Acta2* (p=0.032), *Col1a1* (p=0.04), *Col1a2* (p=0.016), and *Timp1* (p=0.009) in chronic CCl₄ injured livers at 3 week (pre-treatment), 8 week and \pm therapeutic administration of IT-603 (from weeks 3-8). Data are mean \pm s.e.m. in n=4 control mice 7 experimental mice/group. (c,e) P values were calculated using one-way ANOVA with Tukey post-hoc t-test. (d,f) P values were calculated using two-way ANOVA with Tukey post-hoc t-test (*P<0.05, **P<0.001).



Extended data Fig 10: IT-603 attenuates fibrosis in ex vivo human tissues slice models of liver and kidney fibrosis.

(a) Diagrams show the experimental timelines of TGFβ1 induced fibrosis in ex vivo normal human liver and kidney precision cut slices (PCS). (b) Representative images of CD68 stained liver and kidney tissue slices. (c) Representative images and histological quantification of Picrosirius red stained fibrotic kidney slices ± IT-603 therapy ($p < 0.0001$). Representative images and histological quantification of αSMA stained fibrotic kidney slices ± IT-603 therapy ($p < 0.0001$). Red line denotes the value for the T=0 slice. (e) Quantification of soluble collagen released from fibrotic kidney slices ± IT-603 therapy ($p = 0.0015$). (f)

Quantification of the neo-epitope pro C3 released from fibrotic kidney slices \pm IT-603 therapy ($p=0.0493$). (g) Graph showing average LDH release in the media expressed as a percentage (%) of positive control (LDH levels in media from a PCS where maximal death was induced by multiple freeze/thaws – normalized to media volume). (IT-603 $p=0.023$ and IT-603+TGF β 1 $p=0.02$). Images representative of $n=3$ independent slice experiments. Data are mean \pm s.e.m. and representative of slices generated from 3 independent donors performed in duplicate. Scale bars equal 100 microns. P values were calculated using two-way ANOVA with Tukey post-hoc t-test (* $P<0.05$, ** $P<0.01$, *** $P<0.001$ and **** $P<0.0001$).